



OPEN ACCESS

EDITED BY

Ivan P. Damians,
Universitat Politècnica de
Catalunya-BarcelonaTech (UPC), Spain

REVIEWED BY

Anna Ramon Tarragona,
Universitat Politècnica de Catalunya, Spain
Claire Watson,
Quintessa, United Kingdom

*CORRESPONDENCE

Maarten W. Saaltink,
✉ maarten.saaltink@upc.edu

RECEIVED 28 March 2025

ACCEPTED 07 May 2025

PUBLISHED 22 May 2025

CITATION

Chaparro MC and Saaltink MW (2025)
Modelling reactive transport in unsaturated
concrete under evaporation and
condensation processes.
Front. Built Environ. 11:1601568.
doi: 10.3389/fbuil.2025.1601568

COPYRIGHT

© 2025 Chaparro and Saaltink. This is an
open-access article distributed under the
terms of the [Creative Commons Attribution
License \(CC BY\)](#). The use, distribution or
reproduction in other forums is permitted,
provided the original author(s) and the
copyright owner(s) are credited and that the
original publication in this journal is cited, in
accordance with accepted academic practice.
No use, distribution or reproduction is
permitted which does not comply with
these terms.

Modelling reactive transport in unsaturated concrete under evaporation and condensation processes

M. Carme Chaparro¹ and Maarten W. Saaltink^{2*}

¹CSD Engineers AG, Aarau, Switzerland, ²Department of Civil and Environmental Engineering, Universitat Politècnica de Catalunya (UPC), Barcelona, Spain

El Cabril is the low- and intermediate-level radioactive waste disposal facility in Spain. Water is collected from the drains situated in the concrete cells storing radioactive waste, indicating flow of water into these concrete cells. 2D numerical models, together with temperature and humidity measurements, suggested that this flow of water was caused by a combination of thermo-hydraulic processes occurring in the unsaturated concrete, such as capillary rise from the groundwater, evaporation, and condensation due to temperature gradients caused by seasonal temperature fluctuations outside. The objective of this work is to study the effect of these processes on the mineralogy of the concrete. Therefore, 1D reactive transport models have been developed following the 2D thermo-hydraulic conceptual model. When minerals are controlled by fast kinetics, the model results show that the cement phases precipitate and dissolve, clearly following the yearly fluctuations of condensation and evaporation. However, when minerals are controlled by slow kinetics, the reactions are less affected by the hydraulic processes. The models suggest that precipitation-dissolution could be particularly important near the air gap in the concrete, where water condenses and evaporates more easily.

KEYWORDS

reactive transport, multiphase flow, concrete, Retraso-Code_Bright, numerical model

1 Introduction

Concrete is a porous material where, in unsaturated conditions, three main phases coexist: the solid phase, the gas phase, and the pore solution. The solid phase consists of aggregates of different sizes and the cement paste. The cement paste is composed mainly of C-S-H (calcium silicate hydrate), portlandite, ettringite, and hydrated calcium aluminate phases (primarily monosulfate and monocarbonate), along with smaller amounts of other hydration products (Taylor, 1997). Typically, the aggregates have less reactivity compared to the strong reactivity of the cement paste (Samson and Marchand, 2007). The pore solution, characterized by its high alkalinity (pH around 13), mainly comprises species such as OH⁻, Na⁺, K⁺, Ca²⁺ and SO₄²⁻ (Lothenbach and Winnefeld, 2006; Samson and Marchand, 2007).

Concrete is widely used in various architectural and engineering structures, including buildings, bridges, and barriers for radioactive waste storage. These structures are exposed to environmental conditions where air temperature and relative humidity vary over time, causing changes in temperature and humidity within the concrete. Since concrete is a reactive material, it can be damaged, and its service life reduced by exposure to temperature

and relative humidity variations due to processes involving water flow, solute transport, heat transport, evaporation, and condensation inside the concrete. Temperature gradients are one of the key factors controlling the processes interacting with concrete exposed to natural environments (Chaparro and Saaltink, 2016; Min et al., 2017; Isteita and Xi, 2017).

In unsaturated cementitious materials, experiments simulating environmental changes in temperature and humidity have been reported to study their effects on concrete. These findings demonstrate that temperature is the main factor influencing the internal relative humidity in concrete (Andrade et al., 1999; Min et al., 2017). As the temperature gradient increases, moisture transport inside concrete augments, leading to increased concrete damage (Min et al., 2017). However, these studies did not investigate changes in the mineralogy of the concrete. To simulate the effect of climate changes on concrete microstructure, El-Turki et al. (2010) conducted experiments on lime mortars exposed to wetting and drying cycles, although they did not account for temperature gradients. Their results suggest the dissolution and re-precipitation of C-S-H during each cycle. Recrystallization of C-S-H and portlandite due to residual unreacted clinker has also been observed by Chapwanya et al. (2009) and Chaparro et al. (2017) in saturated concrete.

In unsaturated porous media, temperature gradients can cause the diffusion of vapour with evaporation at the hot side and condensation at the cold side (Chaparro and Saaltink, 2016). Numerical models have been used to understand processes involving water flow, heat transport, evaporation, and condensation in concrete (Bažant and Najjar, 1972; Häupl et al., 1997; Lü, 2002; Liu et al., 2004). Our study focuses on El Cabril, the low- and intermediate-level radioactive waste disposal facility in Spain. The radioactive waste is stored in concrete cells. El Cabril motivated this study because, after sealing the cells, tritiated water was collected in drains placed at their centre, indicating water flow inside the cell. In previous works, Chaparro and Saaltink (2016), Chaparro and Saaltink (2022) demonstrated through numerical models that the leakage of water collected in the drains of the cells may be caused by capillary rise from the phreatic level, along with evaporation and condensation produced by temperature gradients inside the concrete due to seasonal fluctuations outside. However, in these previous works, changes in concrete microstructure were not considered. Also, within the framework of El Cabril, Trapote (2015) conducted experiments and reactive transport models simulating evaporation in unsaturated mortar under thermal loads. Although her numerical models predicted the dissolution of portlandite, calcite, and ettringite, and the precipitation of C-S-H, this could not be confirmed experimentally. Nevertheless, in another context, Schwotzer et al. (2010) demonstrated experimentally that a condensed drop of water could alter concrete due to carbonation, leading to progressive deterioration of the concrete both laterally and in depth.

Although the effects of temperature changes on mineralogy have been studied even in unsaturated environments (Samper et al., 2018), no modelling studies have been reported on the geochemistry of concrete affected by temperature gradients along with evaporation and condensation processes under natural conditions. Hence, the objective of this work is to study the effect of these hydraulic processes on the mineralogy of the concrete used to store radioactive

waste at El Cabril, following the conceptual model of Chaparro and Saaltink (2016), Chaparro and Saaltink (2022).

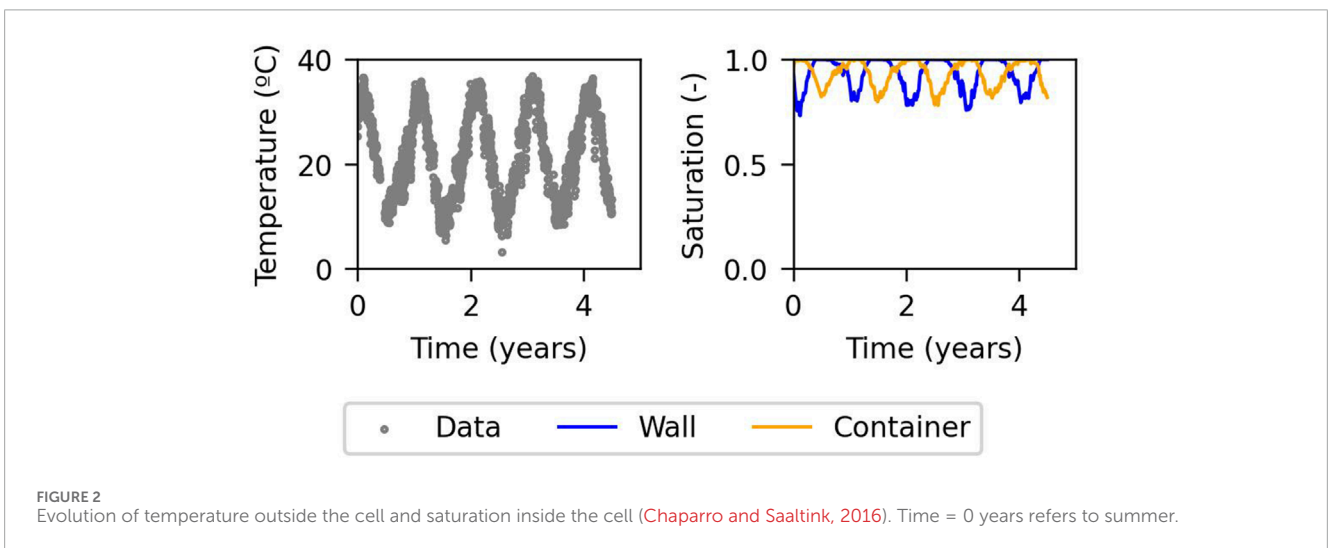
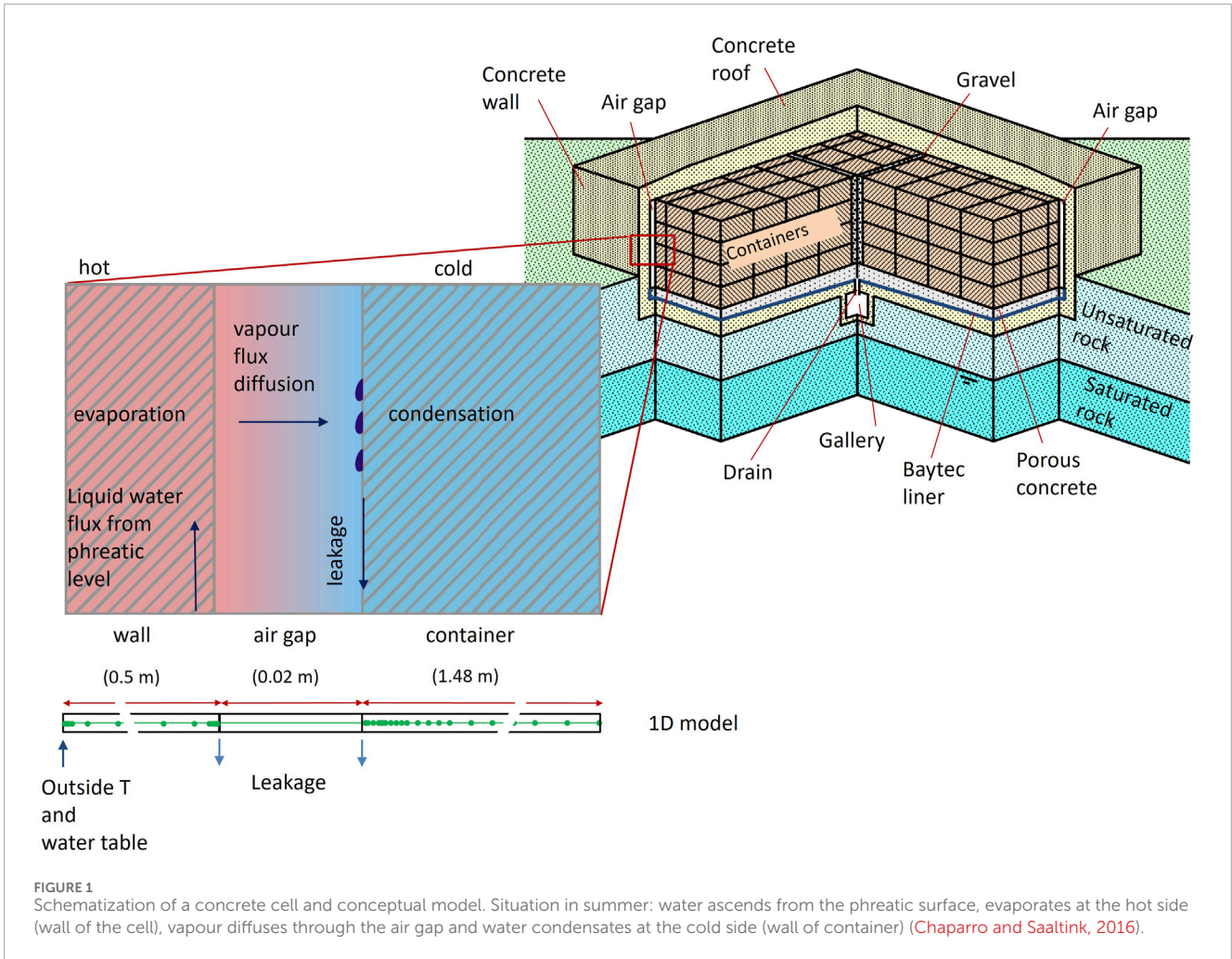
2 Conceptual model

The “El Cabril” radioactive waste facility is situated in southern Spain. It consists of 28 concrete cells designed for waste storage. Each cell measures 19.3 m by 23.8 m by 9 m and has a capacity of 1,000 m³ of radioactive waste (Figure 1). A drainage system is located at the center of each cell and is accessible via a gallery. Initially, the waste is stored in metal drums, which are then placed inside 8 m³ concrete containers filled with mortar. This mortar is composed of two-thirds water and one-third tritiated water. Finally, the sealed containers are positioned within the concrete cells. However, the walls of the containers and the cells do not align perfectly, leaving a small air gap between them. Each cell is embedded 3 m into the underlying rock, while the remaining portion is exposed to atmospheric temperature variations. External temperatures range from 40°C in summer and 5°C in winter (Figure 2). The phreatic level is 4 m below the base of the cells. In the future, once all the cells are filled, a multilayer cover will be installed to protect the entire facility (Gran-Esforzado, 2015).

We follow the same conceptual model used by Chaparro and Saaltink (2016), Chaparro and Saaltink (2022), which considers that water can ascend from the phreatic level to the wall of the cell due to capillary rise through the unsaturated rock. In summer, the wall of the cell is hotter and the wall of the container is colder because the air gap acts as thermal insulation. Thus, water can evaporate from the wall of the cell. This vapour diffuses through the air gap due to the temperature gradient between the wall of the cell and the wall of the container. Water condenses on the wall of the container because of its lower temperature. Consequently, water runs off to the drain. In winter, the wall is colder and the container is hotter. Hence, water evaporates at the container and condenses on the wall. So, again water runs off to the drain. This occurs only in summer and winter because then the temperature difference across the air gap is large enough to produce this phenomenon. Figure 2 shows the evolution of temperature outside the cell measured by sensors (Chaparro and Saaltink, 2016), with the corresponding seasonal fluctuations. This figure also shows the saturation inside the cell calculated by Chaparro and Saaltink (2016), where water evaporates at the side with lower water saturation, and condenses at the side with high water saturations. In this work, the conceptual model also takes into account the chemical reactions in the concrete during the evaporation and condensation processes. To do so, two numerical models have been implemented: one controlled by fast kinetics (where cement phases are practically at equilibrium) and another one controlled by slow kinetics. The model with fast kinetics considers the pore water in equilibrium with the main cement phases, while pore water from the model with slow kinetics is far from equilibrium to those phases.

3 Numerical model

The simulations were carried out using Retraso-CodeBright (Saaltink et al., 2004). This software package



couples CodeBright (Olivella et al., 1996b) to a module for reactive transport modelling, including aqueous complexation reactions, adsorption and precipitation/dissolution of minerals.

3.1 Geometry, materials and mesh

The 1D model is positioned 3.5 m above the base of the cell and has a length of 2 m (Figure 1). It includes the wall of the cell (0.5 m),

TABLE 1 Composition of the ordinary portland cement I-42.5 R/SR.

Component	Quantity (kg/kg)
SiO ₂	1.9 × 10 ⁻¹
Al ₂ O ₃	1.2 × 10 ⁻²
Fe ₂ O ₃	4.5 × 10 ⁻²
CaO	6.6 × 10 ⁻¹
Na ₂ O	9.0 × 10 ⁻⁴
SO ₃	3.1 × 10 ⁻²
K ₂ O	3.3 × 10 ⁻³
CaCO ₃	5.0 × 10 ⁻²
Total	1.0

TABLE 2 Composition of the concrete. Minimum and maximum sizes (mm) of the aggregate and sand are given within parenthesis (Chaparro and Saaltink, 2016; Chaparro et al., 2017).

Component	Quantity
Aggregates (4/16)	1,023 kg/m ³
Sand (0/4)	434 kg/m ³
Sand (0/2)	403 kg/m ³
Ordinary Portland Cement I-42.5 R/SR	400 kg/m ³
Rheobuild 1,222 additive (superplasticizer)	6.5 kg/m ³
Water	175 L/m ³

the air gap (0.02 m), and the container where the waste is stored (1.48 m). The model comprises 63 nodes and 62 one-dimensional elements, with sizes ranging from 0.001 to 0.1 m. The mesh is refined along both sides of the air gap and at the boundary of the wall of the cell. The gap is represented by a single element, with its nodes corresponding to the wall of the cell and the container. The reactions take place in the wall of the cell and container; no reactions occur in the gap.

3.2 Boundary and initial conditions

The initial and boundary conditions used in this numerical model are the same as used in previous works (Chaparro and Saaltink, 2022), which were verified with the measured data from the concrete cells.

The initial temperature of the entire cell is 20°C and the initial liquid pressure is -0.9 MPa.

Following Chaparro and Saaltink (2016), Chaparro and Saaltink (2022), temperature is prescribed and varies with time at the wall of the cell, using the daily average temperature measured

TABLE 3 Primary and secondary phases considered in the numerical model. The initial volumetric fraction and the product $k_m \sigma_m$ are listed for each phase.

Phase	Vol. Frac. (m ³ m ⁻³)	$k_m \sigma_m$ (mol m ⁻³ s ⁻¹)	
		fast kinetics	slow kinetics
Quartz	6.27 × 10 ⁻¹	1.25 × 10 ⁻¹⁴	1.25 × 10 ⁻¹⁴
C-S-H-083	0	1.0 × 10 ⁻⁶	1.0 × 10 ⁻⁶
C-S-H-10	0	1.0 × 10 ⁻⁶	1.0 × 10 ⁻⁶
C-S-H-12	0	1.0 × 10 ⁻⁶	1.0 × 10 ⁻⁶
C-S-H-14	0	1.0 × 10 ⁻⁶	1.0 × 10 ⁻⁶
C-S-H-1667	9.11 × 10 ⁻²	1.0 × 10 ⁻⁶	1.0 × 10 ⁻¹⁰
Portlandite	7.35 × 10 ⁻²	7.24 × 10 ⁻⁸	7.24 × 10 ⁻¹²
Ettringite	3.22 × 10 ⁻²	1.58 × 10 ⁻⁶	7.90 × 10 ⁻¹¹
Calcite	6.10 × 10 ⁻³	1.0 × 10 ⁻⁶	1.0 × 10 ⁻⁸
C-A-S-H-05	0	1.0 × 10 ⁻⁶	1.0 × 10 ⁻⁶
C-A-S-H-10	0	1.0 × 10 ⁻⁶	1.0 × 10 ⁻⁶
C-A-S-H-15	0	1.0 × 10 ⁻⁶	1.0 × 10 ⁻⁶
monocarboaluminate	0	3.16 × 10 ⁻¹¹	3.16 × 10 ⁻¹¹
monosulfoaluminate	0	1.58 × 10 ⁻¹²	1.58 × 10 ⁻¹²

Secondary phases have 0 initial volumetric fraction. Values of $k_m \sigma_m$ of the slow kinetics model have been fitted.

by the sensors situated outside the cell (Figure 2). This boundary condition is applied to the outer boundary of the wall of the cell at the left (Figure 1).

The vertical water flux from and to the groundwater is simulated by a pressure dependent boundary flux taking into account the distance to the groundwater level and the hydraulic conductivity of the concrete (Equations 1–3). This boundary condition is applied to the second node from the wall of the cell, representing the interaction between the groundwater and the concrete porewater occurring at the base of the wall.

$$P_{l,phreatic} = P_{atm} - \rho g z \tag{1}$$

$$\gamma_{wall} = \frac{A \rho k}{L \mu} \tag{2}$$

$$q_{l,phreatic} = \gamma_{wall} (P_{l,phreatic} - P_1) \tag{3}$$

Where $P_{l,phreatic}$ is the liquid pressure at the phreatic level (0.0278 MPa), P_{atm} is the atmospheric pressure (0.1 MPa), z is the distance from the phreatic level to the position of the 1D model (7.5 m). γ_{wall} is the boundary liquid exchange coefficient of the wall (6 × 10⁻⁷ kg s⁻¹m⁻²MPa⁻¹), which takes into account the intrinsic permeability, k , (4.2 × 10⁻¹⁸ m²), liquid density, ρ , (1,000 kg m⁻³),

TABLE 4 Initial composition of the concrete porewater and composition of the groundwater at 20°C, also the imposed constraints to calculate some of these values (equilibrium with solids or charge balance) are indicated. Concentrations of Ca^{2+} , HSiO_3^- and SO_4^{2-} of the concrete pore water with slow kinetics have been fitted to measured concentrations.

Component	Concrete pore water	Concrete pore water	Groundwater
	fast kinetics	slow kinetics	
	(mol L ⁻¹)	(mol L ⁻¹)	
Ca^{2+}	4.69×10^{-3} Portlandite	1.00×10^{-4}	8.38×10^{-4}
HSiO_3^-	1.74×10^{-5} C-S-H-1667	1.74×10^{-5}	1.00×10^{-15}
$\text{Al}(\text{OH})_4^-$	3.54×10^{-5}	3.54×10^{-5}	1.00×10^{-15}
K^+	6.60×10^{-2}	6.60×10^{-2}	1.40×10^{-4}
Na^+	2.53×10^{-2}	2.53×10^{-2}	3.08×10^{-3}
SO_4^{2-}	9.35×10^{-5} Ettringite	1.00×10^{-3}	2.70×10^{-3}
Mg^{2+}	1.00×10^{-15}	1.00×10^{-15}	2.96×10^{-3}
Cl^-	1.00×10^{-15}	1.00×10^{-15}	2.90×10^{-3}
CO_3^{2-}	1.42×10^{-5} Calcite	3.47×10^{-4} Calcite	2.65×10^{-3}
pH	12.85 charge bal.	12.82 charge bal.	7.48

TABLE 5 Equilibrium constants of the minerals taken into account in the numerical model. Reactions are written as the dissolution of 1 mol of mineral in terms of the primary species Ca^{2+} , $\text{SiO}_2(\text{OH})_2^{2-}$, $\text{Al}(\text{OH})_4^-$, OH^- , SO_4^{2-} , CO_3^{2-} , K^+ , Na^+ and Cl^- .

Mineral	Formula	$\log K_{eq}$			
		0 °C	25 °C	60 °C	
Quartz	SiO_2	0.91	0.85	0.83	(a)
C-S-H-083	$2.27\text{SiO}_2 \cdot 1.82\text{Ca}(\text{OH})_2 \cdot 1.82\text{H}_2\text{O}$	-7.16	-7.23	-7.26	(b)
C-S-H-10	$\text{SiO}_2 \cdot \text{Ca}(\text{OH})_2 \cdot 0.86\text{H}_2\text{O}$	-8.44	-8.56	-8.67	(b)
C-S-H-12	$\text{SiO}_2 \cdot 1.2\text{Ca}(\text{OH})_2 \cdot 0.91\text{H}_2\text{O}$	-9.78	-9.94	-10.15	(b)
C-S-H-14	$\text{SiO}_2 \cdot 1.4\text{Ca}(\text{OH})_2 \cdot 0.95\text{H}_2\text{O}$	-11.00	-11.21	-11.52	(b)
C-S-H-1667	$\text{SiO}_2 \cdot 1.67\text{Ca}(\text{OH})_2 \cdot 1\text{H}_2\text{O}$	-12.50	-12.76	-13.19	(b)
Portlandite	$\text{Ca}(\text{OH})_2$	-4.98	-5.19	-5.64	(c)
Ettringite	$\text{Ca}_6\text{Al}_2(\text{SO}_4)_3(\text{OH})_{12} \cdot 26\text{H}_2\text{O}$	-48.37	-44.90	-41.64	(c)
Calcite	CaCO_3	-8.40	-8.48	-8.80	(a)
C-A-S-H-05	$(\text{CaO})_1(\text{Al}_2\text{O}_3)_{0.025}(\text{SiO}_2)_1(\text{H}_2\text{O})_{1.2}$	-10.48	-9.37	-8.74	(d)
C-A-S-H-10	$(\text{CaO})_1(\text{Al}_2\text{O}_3)_{0.05}(\text{SiO}_2)_1(\text{H}_2\text{O})_{1.2}$	-10.61	-9.30	-8.66	(d)
C-A-S-H-15	$(\text{CaO})_1(\text{Al}_2\text{O}_3)_{0.075}(\text{SiO}_2)_1(\text{H}_2\text{O})_{1.2}$	-10.34	-9.11	-8.73	(d)
Monocarboaluminate	$\text{Ca}_4\text{Al}_2\text{CO}_3(\text{OH})_{12} \cdot 5\text{H}_2\text{O}$	-32.65	-32.65	-30.78	(c)
Monosulfoaluminate	$\text{Ca}_4\text{Al}_2\text{SO}_4(\text{OH})_{12} \cdot 6\text{H}_2\text{O}$	-30.10	-30.10	-28.91	(c)

a) EQ3/6 database (Wolery et al., 1990), b) Kulik and Kersten (2001), c) cemdata07 database (Matschei et al., 2007) and d) Myers et al. (2015).

TABLE 6 Secondary species with their equilibrium constants ($\log K_{eq}$) taken into account in the numerical model [EQ3/6 database, [Wolery et al. \(1990\)](#)].

Formula	$\log K_{eq}$		
	0 °C	25 °C	60 °C
Al ³⁺	34.71	33.83	33.23
Al(OH) ₆ SiO ⁻	1.94	1.25	0.70
Al(OH) ₃ (aq)	8.87	8.00	7.17
Al(OH) ₂ ⁺	16.26	15.94	15.60
AlOH ²⁺	25.62	24.85	24.27
AlSiO(OH) ₃ ²⁺	28.24	27.10	26.44
AlSO ₄ ⁺	31.77	30.82	29.84
AlSO ₄ ⁻²	29.89	28.93	27.88
CaCO ₃ (aq)	-3.13	-3.33	-3.68
CaOH ⁺	-1.06	-1.14	-1.37
CaSO ₄ (aq)	-2.07	-2.11	-2.27
CaSiO ₂ (OH) ₂	-4.60	-4.60	-4.60
CaSiO(OH) ₃ ⁺	-0.27	-0.53	-0.59
HCO ₃ ⁻	4.31	3.67	2.90
CaHCO ₃ ⁺	3.22	2.62	1.74
CO ₂ (aq)	12.67	11.32	9.66
KOH(aq)	-0.48	0.46	1.43
KSO ₄ ⁻	-0.89	-0.88	-0.99
NaCO ₃ ⁻	-0.81	-0.51	-0.05
NaOH(aq)	0.15	0.18	0.17
NaSO ₄ ⁻	-0.77	-0.82	-0.91
NaHCO ₃ (aq)	3.95	3.51	3.02
HSO ₄ ⁻	13.22	12.02	10.58
SiO(OH) ₃ ⁻	0.92	0.66	0.61
SiO ₂ (aq)	5.54	4.85	4.30

Reactions are written as the reaction of 1 mol of secondary species in terms of the primary species Ca²⁺, SiO₂(aq), Al(OH)₄⁻, H⁺, SO₄²⁻ and CO₃²⁻.

width of the wall, A , (0.5 m), distance from the base of the cell to the position of the 1D model, L , (3.5 m), and liquid viscosity, μ , (1×10^{-9} MPa s). $q_{l,phreatic}$ is the flow from/to the phreatic level ($\text{kg m}^{-2}\text{s}^{-1}$).

A leakage boundary condition is applied to the air gap between the wall and the container, allowing water to leave the cell only when liquid pressure exceeds atmospheric pressure. This represents the

leakage to the drain (Equation 4; Figure 1).

$$\begin{cases} q_{l,leakage} = \gamma_1 (P_{atm} - P_1) & \text{if } P_1 \geq P_{atm} \\ q_{l,leakage} = 0 & \text{if } P_1 < P_{atm} \end{cases} \quad (4)$$

Where $q_{l,leakage}$ is the leakage rate of condensed water. Water leaves this boundary if the liquid pressure is higher than the atmospheric pressure, and the concrete is fully saturated. γ_1 is a coefficient that has been given a very high value (10 kg/m²/s/MPa) so that liquid pressure hardly exceeds atmospheric pressure.

3.3 Thermo-hydraulic system

Retraso-CodeBright solves the balance equations for water, air, and energy. The water balance takes into account unsaturated flow and vapour diffusion affected by temperature as detailed by [Olivella et al. \(1994\)](#).

The thermo-hydraulic parameters of the concrete used in this model are the same as those used by [Chaparro and Saaltink \(2016\)](#). The porosity is 0.17, the intrinsic permeability is 4.2×10^{-18} m², the solid thermal conductivity is $1.56 \text{ W m}^{-1}\text{K}^{-1}$ for the concrete wall and $3 \text{ W m}^{-1}\text{K}^{-1}$ for the concrete containers. The retention curve (Equation 5) is simulated using the van Genuchten model corrected for temperature changes [Olivella et al. \(1996a\)](#):

$$S = \left(1 + \left(\frac{P_g - P_l}{P_0 \frac{\sigma_T}{\sigma_0}} \right)^{\frac{1}{1-m}} \right)^{-m} \quad (5)$$

where S is the water saturation, P_g and P_l are the gas and liquid pressure respectively (MPa), P_0 is the entry pressure with a value of 3 MPa, m is a shape parameter with a value of 0.34, σ_0 is the surface tension at 20°C (0.072 N/m), and σ_T is the surface tension at temperature T .

The van Genuchten model is also used for the relative permeability as a function of saturation using the same value for m as that of the retention curve (Equation 6).

$$k_{rl} = \sqrt{S} \left(1 - \left(1 - S^{1/m} \right)^m \right)^2 \quad (6)$$

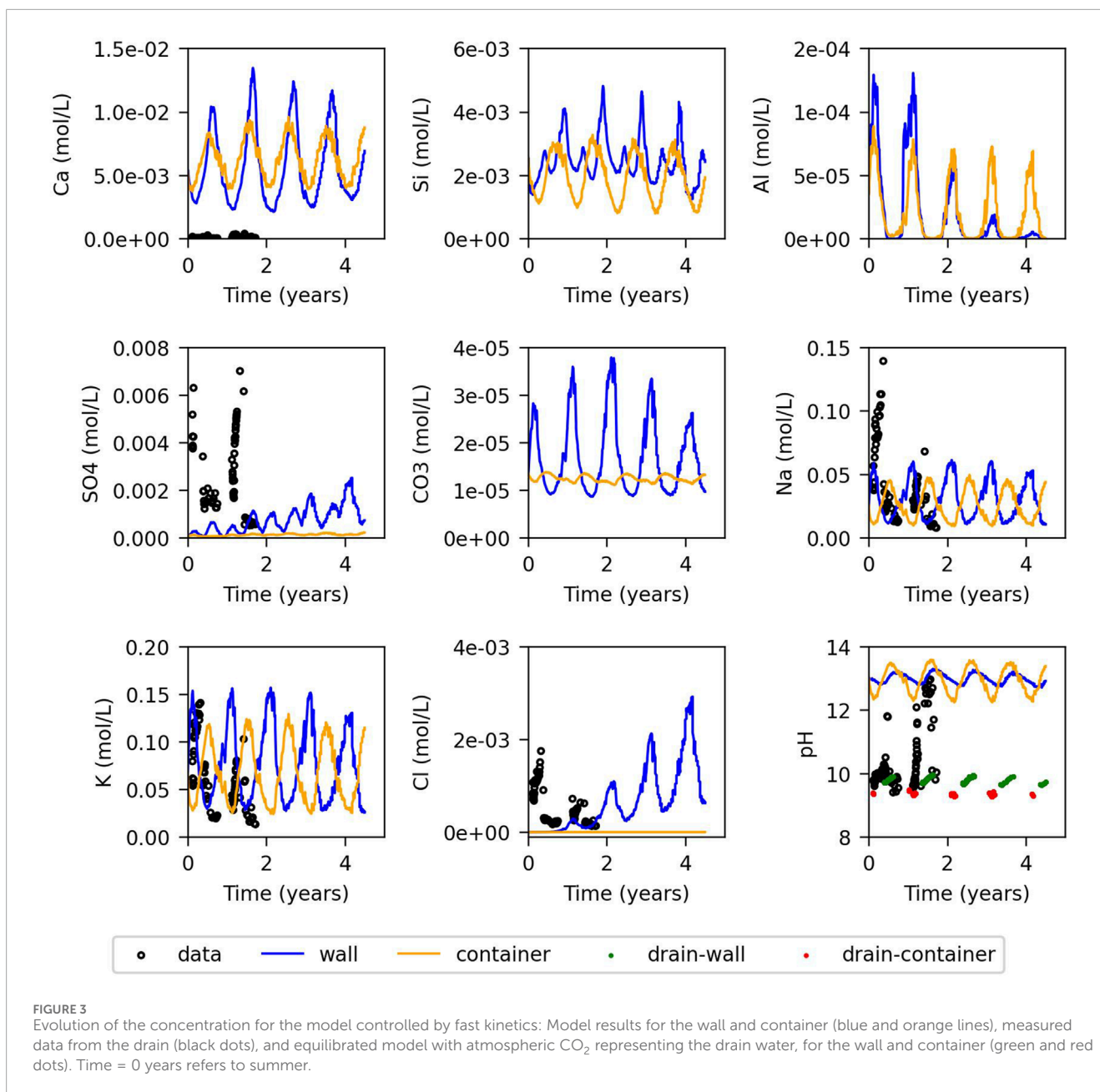
where k_{rl} is the relative permeability of the liquid phase.

For more details regarding the thermo-hydraulic parameters used in this model, we refer to [Villar et al. \(2009\)](#), [Chaparro et al. \(2015\)](#), and [Chaparro and Saaltink \(2016\)](#).

3.4 Geochemical system

3.4.1 Concrete composition

The concrete used to build the cells for storing radioactive waste was manufactured at El Cabril (Spanish Nuclear Waste Management Company). The numerical model starts when the structure was approximately 13 years old. [Table 1](#) provides the cement composition used to make the concrete, and [Table 2](#) gives the concrete composition ([Chaparro and Saaltink, 2016](#); [Chaparro et al., 2017](#)). The cement paste considered in the numerical model is composed of C-S-H gel, portlandite, ettringite, and calcite as primary phases. Monosulphate or other minor phases are not considered because they were not found by X-ray diffraction, which was analysed in a sample with the same composition as that used

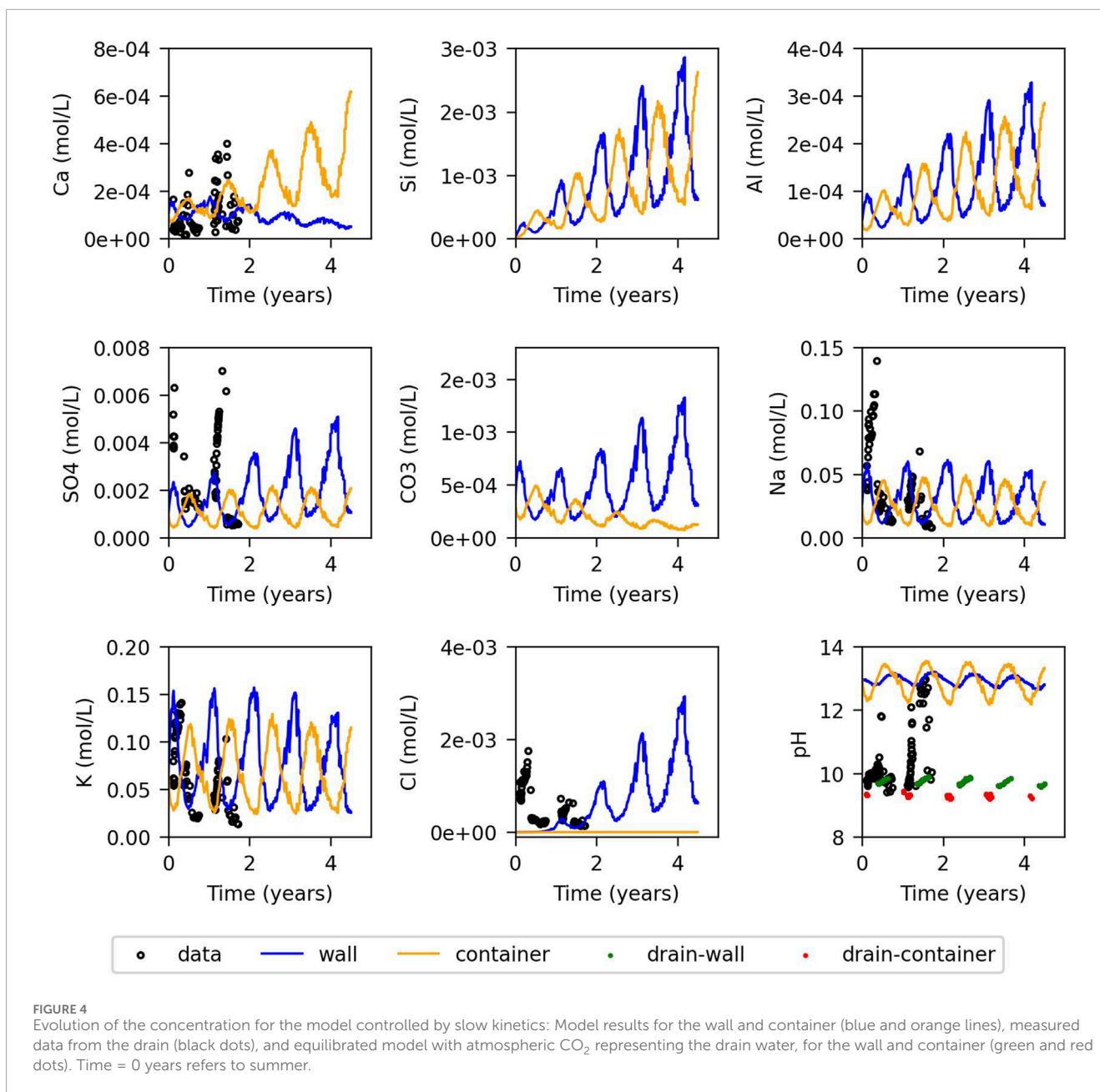


for the cells. The numerical model assumes that aggregates are composed only of quartz, as it is the main component. The C-S-H gel is considered a solid solution with varying Ca/Si ratios. It is modelled assuming five pure minerals with Ca/Si ratio ranging from 0.83 to 1.67. C-S-H-1667 is used as the primary phase and the others as secondary phases. C-A-S-H is also considered a solid solution, with 3 phases having a Ca/Si ratio of one and Al/Si ratios equal to 0.05, 0.10, and 0.15 (Myers et al., 2015). All C-A-S-H phases are considered secondary phases. The volumetric fractions of the primary phases (Table 3) were calculated from the cement and concrete composition.

3.4.2 Water composition

Table 4 shows the chemical composition of the initial concrete pore water and the groundwater used in the numerical model.

The composition of the groundwater corresponds to the measured chemical data from a well located approximately 300 m from the concrete cell storing the radioactive waste, with a phreatic level between 4 and 5 m. As there are no data available on the chemical composition of the groundwater entering the cell, the chemical composition of this well is used instead. Two chemical compositions are considered for the initial concrete pore water according to two different conceptual models. The model referred to as fast kinetics considers the Ca, Si, SO₄ and CO₃ of the concrete pore water at equilibrium with portlandite, C-S-H-1667, ettringite and calcite respectively (Table 4). The other components (K, Na, Al) are calibrated according to the measured water composition. The pH is calculated assuming zero charge balance. In the model referred to as slow kinetics, the CO₃ in the concrete pore water is at equilibrium with calcite, and the other components were adjusted to fit the model



with the composition of the water collected at the drain. The pH is calculated assuming charge balance as well.

3.4.3 Thermodynamic data

The thermodynamic data used in the numerical models depend on the temperature. Table 5 shows the thermodynamic data at different temperatures (0, 25 and 60 °C) for the primary and secondary minerals. Data for calcite and quartz are taken from EQ3/6 database (Wolery et al., 1990). The data of the discretised C-S-H gel are taken from Kulik and Kersten (2001). The thermodynamic data for portlandite, ettringite, monosulfaluminate and monocarboaluminate are from cemdata07 database (Matschei et al., 2007), and for C-A-S-H from Myers et al. (2015). Table 6 displays the aqueous complexation reactions, which were selected using speciation calculation with PHREEQC

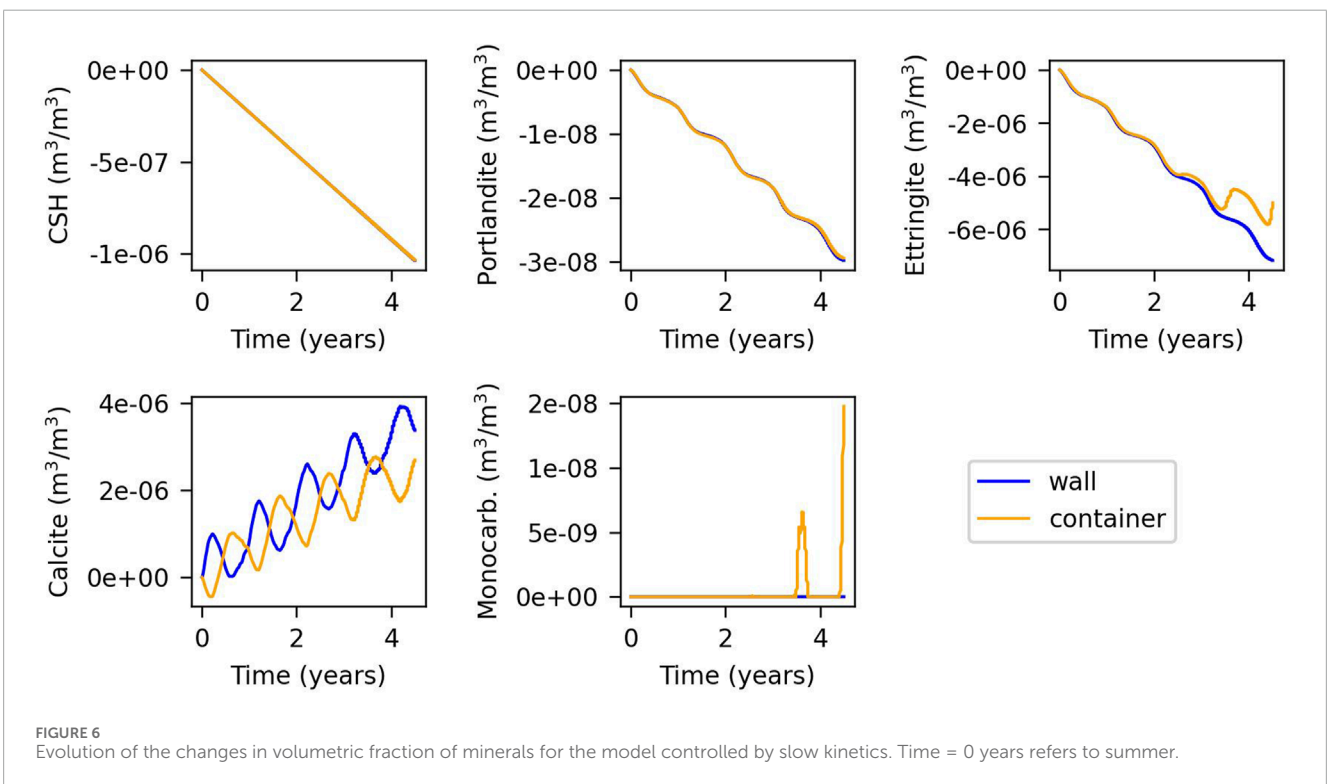
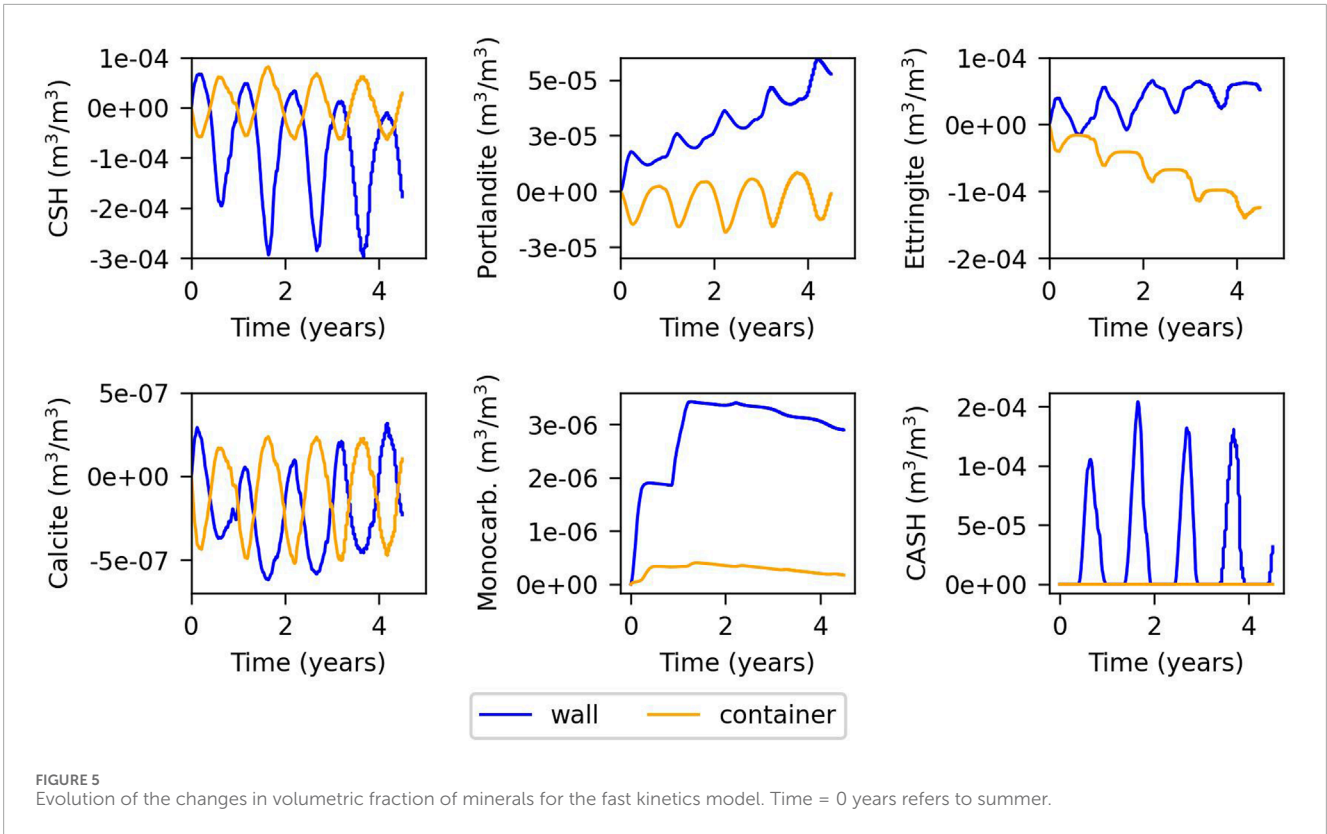
(Parkhurst and Appelo, 1999). The thermodynamic data are taken from EQ3/6 database (Wolery et al., 1990).

3.4.4 Reaction rates

A kinetic approach is used for the dissolution-precipitation of mineral phases, although sometimes the reaction is fast enough to be practically at equilibrium. The form of the rate law, Equation 7, is from Lasaga (1984).

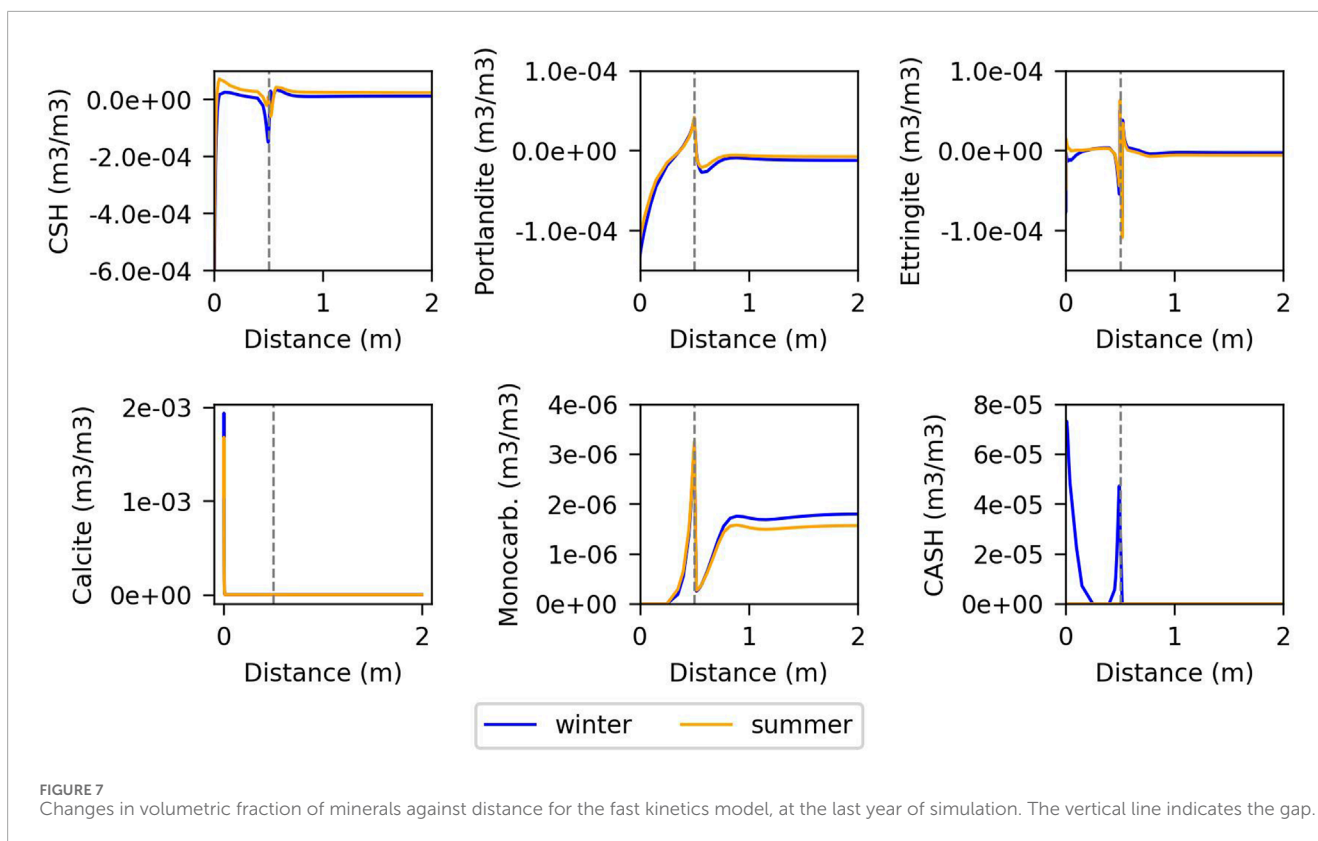
$$r_m = k_m \sigma_m (\Omega_m - 1) \quad (7)$$

Here, r_m is the mineral dissolution-precipitation rate (mol m⁻³ s⁻¹), k_m is the kinetic rate constant (mol m⁻² s⁻¹), σ_m is the surface area (m²m⁻³), and Ω_m is $\frac{IAP}{K}$, where IAP is the ionic activity product and K is the equilibrium constant (ionic activity product at equilibrium).



For the model with fast kinetics, large values of the surface areas for cement phases and secondary phases are used ($k_m \sigma_m$ between $1 \cdot 10^{-6}$ and $1 \cdot 10^{-8} \text{ mol m}^{-3} \text{ s}^{-1}$), leading to local equilibrium

with respect to those phases. In the model with slow kinetics, the surface areas for portlandite, C-S-H, ettringite, and calcite are reduced (Table 3). The kinetic constants are the same as used by



Chaparro et al. (2017). The rate law used for quartz, Equation 8, in both conceptual models, is taken from Bandstra et al. (2008).

$$r_m = k_m \sigma_m a_{H^+}^{-0.4} \quad (8)$$

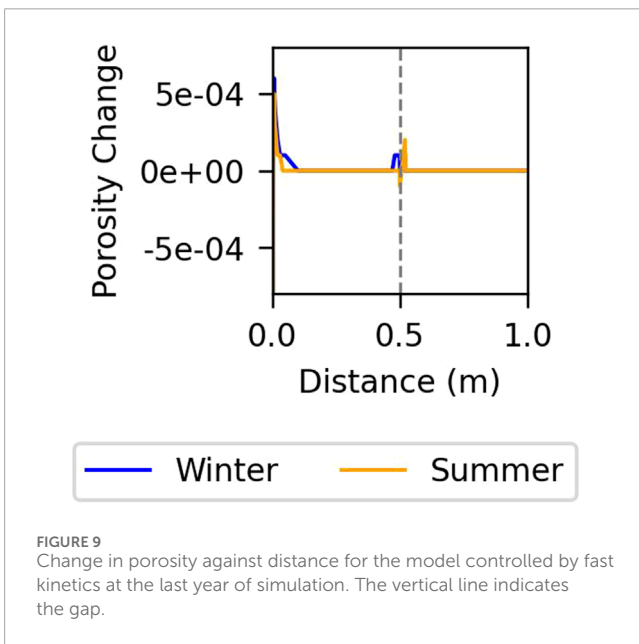
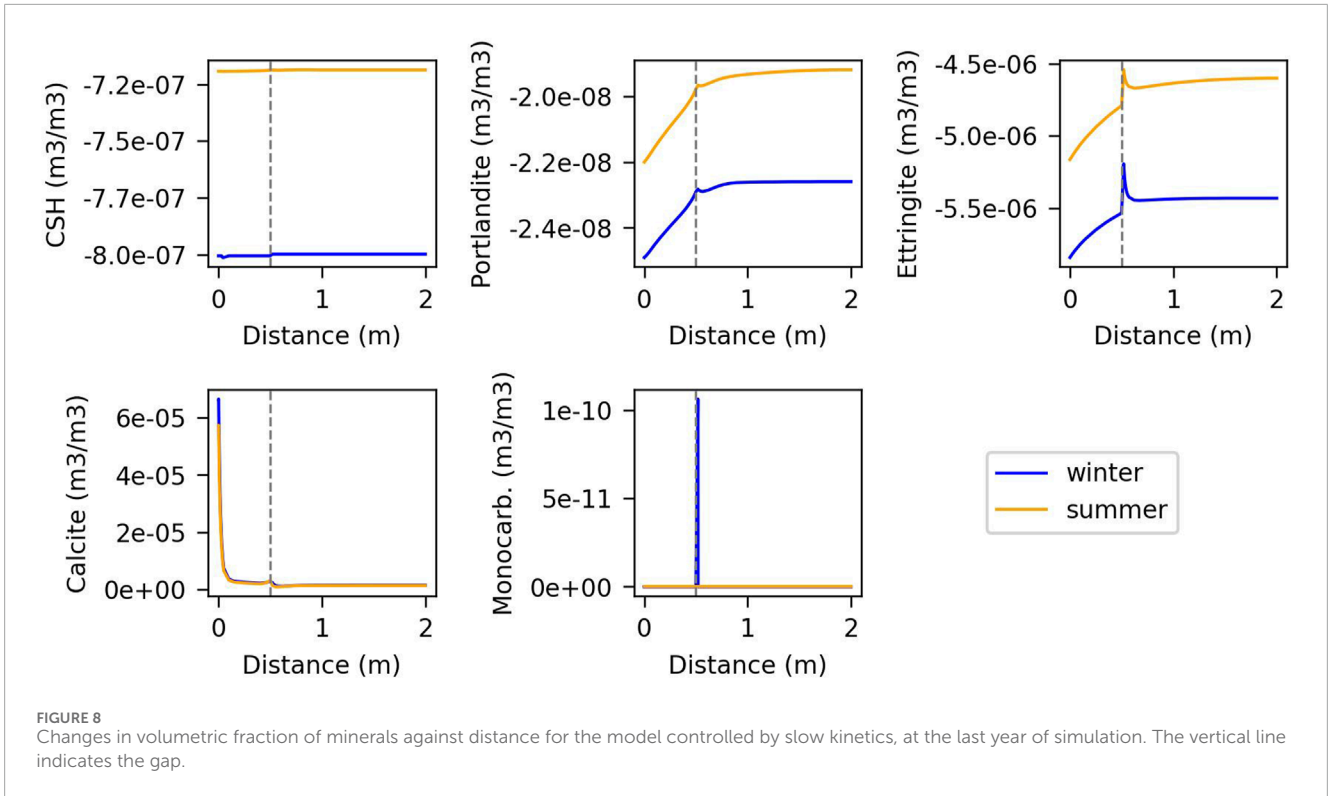
Where a is the activity and H^+ protons.

4 Results and discussion

4.1 Water composition

The evolution of measured concentrations of several chemical components in the water collected in the drain is compared with the model results in Figures 3, 4, for those components with measurements. Otherwise, only model results are presented. Figure 3 corresponds to the model with fast kinetics, and Figure 4 to the one with slow kinetics. In both models the fluctuating temperature at the outside leads to fluctuating saturation, as shown in Figure 2, due to evaporation and condensation discussed in Section 2. This affects also chemical composition and reactions. Concentrations are higher on the hotter side - during summer at the wall of the cell and during winter at the wall of the container - due to evaporation. Calcium concentration is overestimated when portlandite is assumed to be at equilibrium, indicating that in reality the concentrations in the cement pore water are not in equilibrium with the cement phases [also observed by Chaparro et al. (2017)]. The model with fast kinetics initially assumes equilibrium with portlandite, which is clearly not the case. Therefore, the chemical composition of the initial concrete pore water for the fast kinetics

model was adjusted to match the concentration measured in the water collected in the drain. Additionally, the products of kinetic rate constant and surface area ($k_m \sigma_m$) of portlandite, C-S-H gel, ettringite, and calcite had to be reduced to achieve better fits. The reduction in surface area of portlandite, ettringite and C-S-H could indicate carbonation (Johannesson and Utgenannt, 2001; Šavija and Luković, 2016). The cell was exposed to atmospheric CO_2 and rainwater for 4 years after construction before being filled with radioactive waste and isolated from atmospheric CO_2 . During this period, carbonation may have occurred, and the pore water may have been affected by groundwater from capillarity. Better fits are obtained for SO_4 in the model with slow kinetics due to ettringite dissolution. However, this model does not perfectly fit the measured concentration of SO_4 . This discrepancy can be explained by the groundwater composition used by the model, which does not accurately represent the actual composition entering the cell. Due to a lack of data, the composition of groundwater from a well nearby to the waste cell was used instead. Both models show identical results for K, because this chemical component is conservative (that is, it is not involved in precipitation-dissolution) and both models have the same concentration for initial concrete pore water and inflowing groundwater (Table 4). Being conservative, its concentration is mainly controlled by evaporation and condensation with concentrations that rise when water evaporates (at the wall during summer and at the container during winter) and drop when it condenses (at the container during summer and at the wall during winter). As the models show good fits, they reproduce well these processes. As Na is conservative as well, the same holds for this chemical component. Though Cl is also conservative, its behaviour is



slightly different, because, contrarily to Na and K, its initial concrete pore water concentration is low and practically all Cl originates from the groundwater. This only affects concentrations at the wall and is reproduced well by both models except for the first summer. The pH calculated by the numerical models oscillates between 12.5 and 13.4 due to changes in water saturation. Neither model reproduces the measured pH in the drain accurately. The models predict a pH around 13, whereas the measured pH is around 10. The water

collected in the drain may have been exposed to atmospheric CO₂ before or during pH measurement, which could lower the pH from 13 to 10 (Pu et al., 2012). The numerical models do not account for atmospheric CO₂ because they assume the cell is isolated from the atmosphere. Therefore, a calculation using Phreeqc (Parkhurst and Appelo, 1999) and Python was conducted to support this hypothesis. The initial water composition calculated by the numerical model was equilibrated with atmospheric CO₂. The results confirm that the pH drops from 12.99 to 9.78 when water is at equilibrium with atmospheric CO₂. The pH of the measured data shows a range from 10 to 13 approximately. This variation suggests that not all samples were exposed for sufficient time to reach equilibrium with atmospheric CO₂.

4.2 Mineral variation

Figures 5, 6 depict the evolution of the volumetric fractions for the model with fast and slow kinetics, respectively. In the model with fast kinetics, the results show distinct seasonal variations in mineral fractions corresponding to fluctuations in external temperature. During summer, portlandite, C-S-H, ettringite, and calcite precipitate on the wall of the cell due to evaporation, while they dissolve in the container due to condensation. In winter, the opposite occurs: portlandite, C-S-H, and calcite dissolve in the wall and precipitate in the container. C-A-S-H-05 precipitates alongside portlandite and C-S-H dissolution, reversing when they precipitate. C-A-S-H-05 precipitates exclusively in winter and only on the cell wall. Monocarboaluminate precipitates minimally in the container but slightly more in the cell wall, possibly influenced by capillary

groundwater infiltration. Other secondary phases considered do not precipitate.

In contrast, the model with slow kinetics exhibits less dissolution and precipitation of portlandite, C-S-H, and ettringite. Temperature-driven fluctuations are less pronounced, since the chemical composition is far from equilibrium. Therefore, concentration changes due to condensation/evaporation do not have an important effect on precipitation-dissolution rates as shown by Equation 7. In contrast, calcite dissolution and precipitation remain significant and follow annual temperature cycles, reflecting equilibrium conditions. There is no precipitation of C-A-S-H, and monocarboaluminate appears in the container after 3.5 years, primarily in winter, probably due to increased ettringite dissolution from the preceding summer.

Figures 7, 8 illustrate the changes in volumetric fraction of minerals versus distance for summer and winter in models with fast and slow kinetics, respectively. The second node from the outer boundary represents the interaction between groundwater and concrete, which provokes dissolution of C-S-H and portlandite, and strong precipitation of calcite. In reality, this first contact with the groundwater and the concrete porewater is at the base of the wall of the cell. The gap between the wall of the cell and the container is at 0.5 m. In the model with fast kinetics, there is generally more dissolution and precipitation near the gap, where the temperature gradient and vapour diffusion are higher. Portlandite, C-S-H gel, ettringite, and calcite exhibit similar behaviour in both winter and summer. However, C-A-S-H appears predominantly in summer and primarily in the wall, dissolving completely in winter due to the dissolution of portlandite and C-S-H in summer and their precipitation in winter. Monocarboaluminate precipitates near the gap and in the container.

In contrast, the model controlled by kinetics shows lower dissolution and precipitation of portlandite, C-S-H, and ettringite, but slightly higher calcite precipitation near to the gap ($1 \times 10^{-7} \text{ m}^3 \text{ m}^{-3}$ in the fast kinetics model and $3 \times 10^{-6} \text{ m}^3 \text{ m}^{-3}$ in the slow kinetics model). Monocarboaluminate precipitates only in the container near the gap. This model is less affected by evaporation/condensation processes that take place near to the gap.

4.3 Porosity

Figure 9 depicts the porosity versus distance in the fast kinetics model. The slow kinetics model predicts no perceptible porosity changes. In the fast kinetics model, although porosity remains relatively stable, there is a slight impact at the second node from the outer boundary due to the interaction between the groundwater and the concrete, and near the air gap due to evaporation and condensation processes. These trends are consistent across both winter and summer conditions.

5 Conclusion

Reactive transport models were developed to investigate the impact of chemical reactions occurring within concrete due to evaporation and condensation processes. The model results demonstrate that the concentration of water collected in the

drain varies with temperature fluctuations outside the cells. Concentrations are higher on the hotter side due to evaporation and lower on the colder side because of condensation. The model controlled by slow kinetics better reproduces the measured concentrations, suggesting that the initial pore water was not initially at equilibrium with cement phases, probably due to exposure to atmospheric conditions before sealing. The pH observed in samples is around 10, which may be attributed to contact with atmospheric CO_2 in the drain or during pH measurement.

The model with fast kinetics, approaching local equilibrium, indicates that portlandite, C-S-H, ettringite, and calcite precipitate and dissolve in clear accordance with annual fluctuations in condensation and evaporation. C-A-S-H precipitates when portlandite and C-S-H dissolve, and dissolves when they precipitate. The precipitation and dissolution of monocarboaluminate are influenced by the dynamics of calcite and ettringite in the container, potentially affected by groundwater in the cell wall. In the model with slow kinetics, there is generally less dissolution and precipitation and a diminished impact of annual temperature fluctuations. This suggests that mineral precipitation-dissolution processes are primarily controlled by kinetics rather than by evaporation and condensation.

Minor changes in porosity, observed only in the fast kinetics model, occur mainly near the gap where water can readily evaporate and condense. However, these changes are minimal and can be considered negligible. Therefore, despite ongoing chemical reactions within the cell, the concrete structure does not appear to suffer significant damage. In the future, the installation will be covered by a multilayer cover. This will reduce considerably the temperature oscillations and, hence, evaporation and condensation near the gap. Therefore, we expect porosity changes and mineral precipitation/dissolution to cease after covering and neither to have an important effect during the total lifetime of the repository.

This 1D model is still qualitative. In order to have more quantitative results, the model should be verified and calibrated with measured data from the storage cells. Unfortunately, these data do not exist because the cells have already been closed. A 2D geometry will further improve the model, in order to have more detail on the vertical distribution of the mineral precipitation and dissolution.

Data availability statement

The original contributions presented in the study are included in the article/supplementary material, further inquiries can be directed to the corresponding author.

Author contributions

MC: Writing – review and editing, Writing – original draft. MS: Writing – review and editing, Writing – original draft.

Funding

The author(s) declare that no financial support was received for the research and/or publication of this article.

Acknowledgments

The authors acknowledge ENRESA (Spanish Nuclear Waste Management) for providing the measured data from “El Cabril” used in this study.

Conflict of interest

Author MC was employed by CSD Engineers AG.

The remaining author declares that the research was conducted in the absence of any commercial or financial relationships that could be construed as a potential conflict of interest.

References

- Andrade, C., Sarria, J., and Alonso, C. (1999). Relative humidity in the interior of concrete exposed to natural and artificial weathering. *Cem. Concr. Res.* 29 (8), 1249–1259. doi:10.1016/s0008-8846(99)00123-4
- Bandstra, J. Z., Buss, H. L., Campen, R. K., Liermann, L. J., Moore, J., Hausrath, E. M., et al. (2008). *Appendix: compilation of mineral dissolution rates*. New York, NY: Springer.
- Bažant, Z., and Najjar, L. (1972). Nonlinear water diffusion in nonsaturated concrete. *Matériaux Constr.* 5, 3–20. doi:10.1007/bf02479073
- Chaparro, M. C., and Saaltink, M. W. (2016). Water, vapour and heat transport in concrete cells for storing radioactive waste. *Adv. Water Resour.* 94, 120–130. doi:10.1016/j.advwatres.2016.05.004
- Chaparro, M. C., and Saaltink, M. W. (2022). Tritium transport in non-saturated concrete under temperature fluctuations. *J. Environ. Radioact.* 251–252, 106969. doi:10.1016/j.jenvrad.2022.106969
- Chaparro, M. C., Saaltink, M. W., and Villar, M. V. (2015). Characterization of concrete by calibrating thermo-hydraulic multiphase flow models. *Transp. Porous Media* 109, 147–167. doi:10.1007/s11242-015-0506-9
- Chaparro, M. C., Soler, J. M., Saaltink, M. W., and Mäder, U. K. (2017). Reactive transport models of a high-pH infiltration test in concrete. *Physics and Chemistry of the Earth* 99, 131–141. doi:10.1016/j.pce.2017.01.010
- Chapwanya, M., Stockie, J., and Liu, W. (2009). A model for reactive porous transport during re-wetting of hardened concrete. *J. Eng. Math.* 65 (1), 53–73. doi:10.1007/s10665-009-9268-0
- El-Turki, A., Ball, R. J., Holmes, S., Allen, W. J., and Allen, G. C. (2010). Environmental cycling and laboratory testing to evaluate the significance of moisture control for lime mortars. *Constr. Build. Mater.* 24 (8), 1392–1397. doi:10.1016/j.conbuildmat.2010.01.019
- Gran-Esforzado, M. (2015). “Coupled heat and water flow dynamics in dry soils,” in *Application to a multilayer waste cover*. Universitat Politècnica de Catalunya UPC. Ph.D. thesis.
- Häupl, P., Grunewald, J., Fechner, H., and Stopp, H. (1997). Coupled heat air and moisture transfer in building structures. *Int. J. Heat Mass Transf.* 40, 1633–1642. doi:10.1016/s0017-9310(96)00245-1
- Isteita, M., and Xi, Y. (2017). The effect of temperature variation on chloride penetration in concrete. *Constr. Build. Mater.* 156, 73–82. doi:10.1016/j.conbuildmat.2017.08.139
- Johannesson, B., and Utgenannt, P. (2001). Microstructural changes caused by carbonation of cement mortar. *Cem. Concr. Res.* 31 (6), 925–931. doi:10.1016/s0008-8846(01)00498-7
- Kulik, D., and Kersten, M. (2001). Aqueous solubility diagrams for cementitious waste stabilization systems: II, end-member stoichiometries of ideal calcium silicate hydrate solid solutions. *J. Am. Ceram. Soc.* 84, 3017–3026. doi:10.1111/j.1151-2916.2001.tb01130.x
- Lasaga, A. C. (1984). Chemical kinetics of water-rock interactions. *J. Geophys. Res. Solid Earth* 89 (B6), 4009–4025. doi:10.1029/jb089ib06p04009
- Liu, J., Aizawa, H., and Yoshino, H. (2004). CFD prediction of surface condensation on walls and its experimental validation. *Build. Environ.* 39, 905–911. doi:10.1016/j.buildenv.2004.01.015
- Lothenbach, B., and Winnefeld, F. (2006). Thermodynamic modelling of the hydration of portland cement. *Cem. Concr. Res.* 36 (2), 209–226. doi:10.1016/j.cemconres.2005.03.001
- Lü, X. (2002). Modelling of heat and moisture transfer in buildings: I. model program. *Energy Build.* 34, 1033–1043. doi:10.1016/s0378-7788(02)00021-x
- Matschei, T., Lothenbach, B., and Glasser, F. P. (2007). Thermodynamic properties of portland cement hydrates in the system CaO-Al₂O₃-SiO₂-CaSO₄-CaCO₃-H₂O. *Cem. Concr. Res.* 37 (10), 1379–1410. doi:10.1016/j.cemconres.2007.06.002
- Min, H., Zhang, W., Gu, X., and Černý, R. (2017). Coupled heat and moisture transport in damaged concrete under an atmospheric environment. *Constr. Build. Mater.* 143, 607–620. doi:10.1016/j.conbuildmat.2017.03.163
- Myers, R. J., L’Hôpital, E., Provis, J. L., and Lothenbach, B. (2015). Effect of temperature and aluminium on calcium (alumino)silicate hydrate chemistry under equilibrium conditions. *Cem. Concr. Res.* 68, 83–93. doi:10.1016/j.cemconres.2014.10.015
- Olivella, S., Carrera, J., Gens, A., and Alonso, E. E. (1994). Nonisothermal multiphase flow of brine and gas through saline media. *Transp. Porous Media* 15, 271–293. doi:10.1007/bf00613282
- Olivella, S., Carrera, J., Gens, A., and Alonso, E. E. (1996a). Porosity variations in saline media caused by temperature gradients coupled to multiphase flow and dissolution/precipitation. *Transp. Porous Media* 25, 1–25. doi:10.1007/bf00141260
- Olivella, S., Gens, A., Carrera, J., and Alonso, E. E. (1996b). Numerical formulation for a simulator (CODE_BRIGHT) for the coupled analysis of saline media. *Eng. Comput.* 13 (7), 87–112. doi:10.1108/02644409610151575
- Parkhurst, D. L., and Appelo, C. (1999). User’s guide to PHREEQC (version 2) - a computer program for speciation, batch-reaction, one-dimensional transport, and inverse geochemical calculations. *U. S. Geol. Surv. water-resour. Invest. Rep.*, 99–4259.
- Pu, Q., Jiang, L., Xu, J., Chu, H., Xu, Y., and Zhang, Y. (2012). Evolution of pH and chemical composition of pore solution in carbonated concrete. *Constr. Build. Mater.* 28 (1), 519–524. doi:10.1016/j.conbuildmat.2011.09.006
- Saaltink, M. W., Batlle, F., Ayora, C., Carrera, J., and Olivella, S. (2004). RETRASO, a code for modeling reactive transport in saturated and unsaturated porous media. *Geol. Acta* 2 (3), 235–251.
- Samper, J., Mon, A., Montenegro, L., Cuevas, J., Turrero, M., Naves, A., et al. (2018). Coupled THCM model of a heating and hydration concrete-bentonite column test. *Appl. Geochem.* 94, 67–81. doi:10.1016/j.apgeochem.2018.05.007
- Samson, E., and Marchand, J. (2007). Modeling the transport of ions in unsaturated cement-based materials. *Comput. & Struct.* 85 (23), 1740–1756. doi:10.1016/j.compstruc.2007.04.008
- Šavija, B., and Luković, M. (2016). Carbonation of cement paste: understanding, challenges, and opportunities. *Constr. Build. Mater.* 117, 285–301. doi:10.1016/j.conbuildmat.2016.04.138
- Schwotzer, M., Scherer, T., and Gerdes, A. (2010). Protective or damage promoting effect of calcium carbonate layers on the surface of cement based materials in aqueous environments. *Cem. Concr. Res.* 40 (9), 1410–1418. doi:10.1016/j.cemconres.2010.05.001
- Taylor, H. F. W. (1997). *Cement chemistry*. Thomas Telford Ltd.
- Trapote, A. (2015). *Dissolution kinetics of C-S-H gel and durability of mortar*. Universitat Politècnica de Catalunya UPC. Ph.D. thesis.
- Villar, M., Martín, P., and Barcala, J. (2009). Caracterización del material de cobertera y el hormigón del C.A. El Cabril. *Tech. Rep.* CIEMAT.
- Wolery, T. J., Jackson, K. J., Bourcier, W. L., Bruton, C. J., Viani, B. E., Knauss, K. G., et al. (1990). Current status of the EQ3/6 software package for geochemical modeling. *Chem. Model. Aqueous Syst.* II, 104–116. doi:10.1021/bk-1990-0416.ch008

Generative AI statement

The author(s) declare that no Generative AI was used in the creation of this manuscript.

Publisher’s note

All claims expressed in this article are solely those of the authors and do not necessarily represent those of their affiliated organizations, or those of the publisher, the editors and the reviewers. Any product that may be evaluated in this article, or claim that may be made by its manufacturer, is not guaranteed or endorsed by the publisher.